Science Bulletin 62 (2017) 1173–1176

Contents lists available at ScienceDirect

Science Bulletin

journal homepage: www.elsevier.com/locate/scib

Science Bulletin
www.scibull.com

Short Communication

Single crystalline $CH_3NH_3PbI_3$ self-grown on FTO/TiO_2 substrate for high efficiency perovskite solar cells

Jinjin Zhao [a,b,*], Guoli Kong [a], Shulin Chen [c,h], Qian Li [d], Boyuan Huang [b,e], Zhenghao Liu [b], Xingyuan San [f], Yujia Wang [f], Chen Wang [a], Yunce Zhen [a], Haidan Wen [d], Peng Gao [c,g], Jiangyu Li [b,e,*]

[a] School of Materials Science and Engineering, Shijiazhuang Tiedao University, Shijiazhuang 050043, China
[b] Shenzhen Key Laboratory of Nanobiomechanics, Shenzhen Institutes of Advanced Technology, Chinese Academy of Sciences, Shenzhen 518055, China
[c] Electron Microscopy Laboratory, and International Center for Quantum Materials, School of Physics, Peking University, Beijing 100871, China
[d] X-ray Science Division, Argonne National Laboratory, Lemont, IL 60439, USA
[e] Department of Mechanical Engineering, University of Washington, Seattle, WA 98195-2600, USA
[f] Shenyang National Laboratory for Materials Science (SYNL), Institute of Metal Research, Chinese Academy of Sciences, Shenyang 110016, China
[g] Collaborative Innovation Center of Quantum Matter, Beijing 100871, China
[h] State Key Laboratory of Advanced Welding and Joining, Harbin Institute of Technology, Harbin 150001, China

ARTICLE INFO

Article history:
Received 31 July 2017
Received in revised form 13 August 2017
Accepted 18 August 2017
Available online 21 August 2017

Since its first report in 2009, $CH_3NH_3PbI_3$-based perovskite solar cells (PSCs) have emerged as one of the most exciting developments in the next generation photovoltaic (PV) technologies [1], with its PV conversion efficiency (PCE) rising spectacularly from 3.81% to 22.1% in just 7 years. Such rapid advance is unprecedented in any other PV systems, fueling intense competitions for its PCE record worldwide. While still far away from its theoretical limit, the recent PCE advances in PSCs have slowed down considerably, due to the inevitable defects associated with grains and grain boundaries in polycrystalline perovskites as well as their poor stability. It is thus not surprising that some of recent efforts in PSCs have been shifted toward developing single crystalline perovskite materials.

Initial efforts in single crystalline PSCs have been focused on growing large crystals of $CH_3NH_3PbI_3$ and related materials, which has resulted in observations of carrier diffusion length exceeding 175 μm and carrier lifetime over 262 μs, thanks to much reduced trap state density in single crystals [2–4]. Such exceptional photo-carrier properties of single crystalline perovskites, however, have yet to be translated into gains in their PCEs, since it is rather difficult to integrate single crystals of $CH_3NH_3PbI_3$ and related materials into the device architecture of PSCs, wherein interfaces between the photo-harvesting perovskites and carrier collectors such as TiO_2 are critical. For example, large crystalline wafer of perovskite has been sliced into thin layers to make optoelectronic devices [5], though the corresponding solar cell has a relatively low short-circuit current density (J_{sc}) of 13.5 mA/cm^2, resulting in single crystalline PCEs around 4%. Meanwhile, patterned wafer-scale single crystalline films of $CH_3NH_3PbI_3$ have been reported [6,7], exhibiting PCE of 4.83% recorded in a PSC with a lateral configuration [7]. Recently, hybrid perovskite single crystalline films on a variety of flat substrates have been fabricated via space-confined growth, though their PCEs were not reported [8]. Furthermore, single crystalline $CH_3NH_3PbBr_3$ films have been developed using space-limited inverse temperature crystallization growth, resulting in the highest PCE of 7.11% reported to date among single crystalline PSCs [9]. Here, we report a strategy to self-grow high quality single crystalline perovskite $CH_3NH_3PbI_3$ directly on electron-collecting FTO/TiO_2 substrate, similar to a process reported in Ref. [8] using other substrates, with which n-i-p type of perovskite solar cells were fabricated following a standard procedure. The champion cell exhibits a PCE of 8.78%, and there are still substantial rooms for further improvement, making it promising for the perovskite solar cell applications.

Our single crystalline $CH_3NH_3PbI_3$ was self-grown on the FTO/TiO_2 substrate, as schematically shown in Fig. 1a, wherein the electron-collecting TiO_2 layer consists of mesoporous TiO_2 (m-TiO_2) on top of compact TiO_2 (c-TiO_2). The FTO/TiO_2 substrate was dipped vertically into the $CH_3NH_3PbI_3$ precursor solution with its temperature set at 120 °C, and another parallel FTO/TiO_2 glass, approximately 50–200 μm from the substrate using a Teflon spacer, was dipped into the precursor solution as well to form a controlled gap. The capillary pressure and temperature gradient

* Corresponding authors.
E-mail addresses: jinjinzhao2012@163.com (J. Zhao), jjli@uw.edu (J. Li).

http://dx.doi.org/10.1016/j.scib.2017.08.022

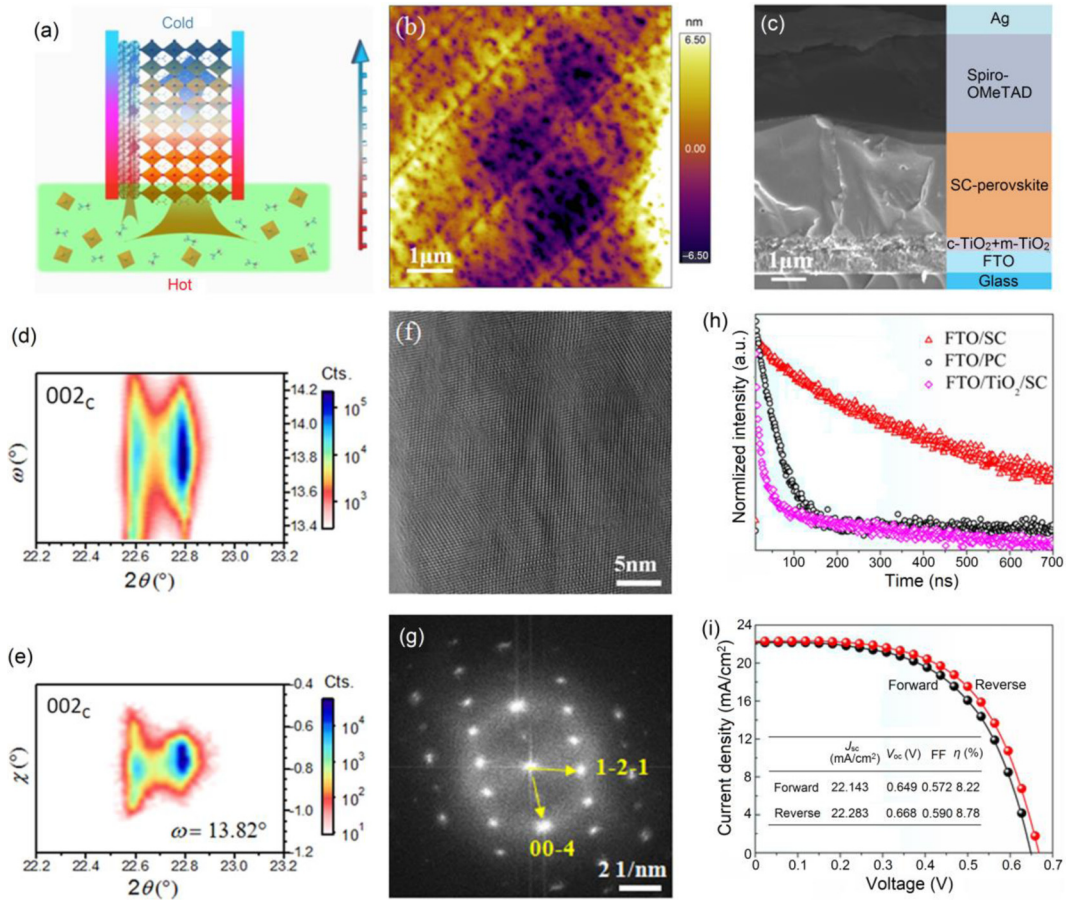

Fig. 1. (Color online) Single crystalline $CH_3NH_3PbI_3$ self-grown on FTO/TiO_2 and glass substrates. (a) Schematic self-growth via temperature gradient and capillary effect. (b) AFM topography mapping of $CH_3NH_3PbI_3$ on glass. (c) Cross-section SEM image of the single crystalline $CH_3NH_3PbI_3$ solar cell. (d), (e) Selected reflections measured from $CH_3NH_3PbI_3$ on FTO/TiO_2 substrate. (f), (g) High resolution transmission electron microscopy (HRTEM) image and the corresponding FFT pattern of single crystalline $CH_3NH_3PbI_3$. (h) Time-resolved photoluminescence (TRPL) of single crystalline (SC) and polycrystalline (PC) $CH_3NH_3PbI_3$ on different substrates. (i) *J-V* curve of the champion cell.

drove the solution upward on the substrate, and the thickness of solution film depends on the gap size that could be adjusted. The growth also occurred on glass or on FTO substrate in the absence of m-TiO_2, as reported in Ref. [8], though at a slower rate, and more details on crystalline growth and experimental methods can be found in Supplementary Information (online). After being taken out of the solution and annealed under 120 °C for 20 min, large scale perovskite $CH_3NH_3PbI_3$ crystal with lateral size over several hundred micrometers was obtained, as shown by the top view and cross-sectional scanning electron microscopy (SEM) image in Figs. S1 and S2 (online). Electron backscatter diffraction (EBSD) taken at four different spots reveal identical Kikuchi patterns (Fig. S2 online), demonstrating their identical crystallographic orientations characteristic of a single crystal. Mapping of atomic force microscope (AFM) topography in Fig. 1b shows smooth surface with root mean square (RMS) roughness around 3.36 nm, and the line feature observed in AFM topography is deemed not an artifact, but may arise from domains of ferroelastic or ferroelectric nature [10,11], as supported by AFM topography of different scan sizes (Fig. S3 online). The cross-sectional SEM images (Figs. S1 and S2 online) reveals a tightly integrated interface between $CH_3NH_3PbI_3$ and FTO/TiO_2 that is important for the PSC devices, and n-i-p type of PSCs consisting of FTO/TiO_2/$CH_3NH_3PbI_3$/Spiro-OMeTAD/Ag were fabricated, with its cross-sectional profile shown by SEM image in Fig. 1c. While the fracture surface is rough, the grain features evident in TiO_2 layer is clearly absent in $CH_3NH_3PbI_3$.

The crystallinity of $CH_3NH_3PbI_3$ sample was examined by X-ray diffraction over large surface region on the scale of hundreds of microns, and the results in Fig. 1d, e illustrate the profiles of two measured reflections denoted in the pseudo-cubic setting. All measured reflections appear to contain multiple split peaks, suggesting a lower-symmetry structure at room temperature. A total of 14 peak positions were extracted and indexed with the Dicvol06 program, yielding a highest-symmetry, orthorhombic unit cell with lattice parameters a = 6.322(4) Å, b = 6.287(2) Å and c = 6.273(2) Å averaged for the probed sample volume. The observation of 002_C-type reflections in the specular condition suggests that the dominant vertical growth direction of $CH_3NH_3PbI_3$ is along the $[0\,0\,1]_C$, and the full width at half maximum (FWHM) of the ω-rocking angle is found to be ~0.2°. The 002_C peaks observed at two distinct 2θ angles but almost identical ω-/χ-angles suggest their association with two types of vertical growth manners rather than the low-symmetry structure twinning. Despite this and the observed overlapping among non-specular reflections, a lack of powder diffraction clearly demonstrates the large, discreet single-crystalline nature of the $CH_3NH_3PbI_3$ sample. This is in contrast to the powder rings observed at 41.23°, 48.8° and a few other angles that arise from the polycrystalline TiO_2 layer (Fig. S4 online), because the $CH_3NH_3PbI_3$ crystals do not fully cover the substrate, as shown by SEM images in Fig. S5 (online), where a few crystals as large as millimeter are seen on the substrate. The detailed in-plane alignment information of the sample is still under

investigation, and the misalignment could explain the averaged orthorhombic structure that is slightly distorted from the usually reported tetragonal unit cell. We thus resort to transmission electron microscopy (TEM) to examine the structure of a single $CH_3NH_3PbI_3$ crystal.

Crystallography and elemental mapping of single crystalline $CH_3NH_3PbI_3$ were examined by HRTEM, scanning transmission electron microscopy (STEM) as well as energy dispersive X-ray spectroscopy (EDX) mappings. Low resolution STEM image of $CH_3NH_3PbI_3$ in Fig. S6a (online) shows a regular polygon outlook, and the corresponding EDX mappings in Fig. S6b–e (online) indicate uniform distribution of C, N, Pb, and I elements. HRTEM image in Fig. 1f reveals well-ordered crystalline lattice, and the corresponding fast Fourier transform (FFT) pattern in Fig. 1g is identified to be tetragonal phase with viewing direction along the [2 1 0] zone axis, as confirmed by the simulated electron diffraction pattern in Fig. S6f (online). The tetragonal phase is consistent with previous report [12] as well as our own powder XRD pattern (Fig. S7 online), and single crystalline nature of $CH_3NH_3PbI_3$ on FTO/TiO_2 is further confirmed by additional TEM images in Fig. S8 (online), wherein two separate areas of a 2 μm-long flake show identical lattice planes and selected area electron diffraction (SAED) patterns.

In order to study exciton diffusion, we employed TRPL to compare the carrier lifetime in polycrystalline $CH_3NH_3PbI_3$ on FTO and single crystalline $CH_3NH_3PbI_3$ on FTO as well as on FTO/TiO_2, as shown in Fig. 1h, monitored at the wavelength of 400 nm. In the absence of electron-collecting TiO_2, the longer carrier lifetime reflects higher exciton concentration and fewer recombination, which is what we observe in the single crystalline $CH_3NH_3PbI_3$ compared to the polycrystalline one, suggesting much reduced defects in the single crystal. When the single crystalline $CH_3NH_3PbI_3$ is deposited on the electron collecting FTO/TiO_2 substrate, on the other hand, the carrier lifetime is reduced substantially due to highly efficient electron extraction by TiO_2, thanks to its good interface with the single crystalline perovskite. Such comparison can be better appreciated by fitting the TRPL decay curves using double exponential equation $I = I_0 + A_1 e^{-t/\tau_1} + A_2 e^{-t/\tau_2}$, with the corresponding fitting parameters listed in Table 1. It is found that the average carrier lifetime of 206.2 ns of single crystalline perovskite is 25.5 times longer than 8.1 ns of polycrystalline one, because exciton lifetime in polycrystal is deteriorated by grain boundaries and defects, which contributes to the increased electron transport resistance and bi-molecular recombination. When put on the FTO/TiO_2 substrate, the carrier lifetime of the single crystal is reduced substantially to 11.2 ns because of efficient electron extraction at TiO_2/perovskite interface. We also compare ultraviolet–visible spectroscopy (UV–vis) absorptions and steady-state photoluminescence (PL) of both single- and poly-crystalline $CH_3NH_3PbI_3$ in Fig. S9 (online), where it is observed that the single crystalline perovskite exhibits an extended absorption band to 870 nm, whereas polycrystalline one has an absorption cutoff at 780 nm. This leads to an estimated optic band gap of 1.50 eV for single crystalline $CH_3NH_3PbI_3$ compared to 1.57 eV for polycrystalline one, consistent with previous report [3]. Correspondingly, the steady PL of single crystalline perovskite red-shifts to 830 from 780 nm of polycrystalline one.

The narrower band gap, higher exciton concentration with less recombination, and highly efficient electron extraction are expected to contribute significantly to the high J_{sc} for the single crystalline PSCs. Indeed, the n-i-p type PSCs consisting of FTO/TiO_2/$CH_3NH_3PbI_3$/Spiro-OMeTAD/Ag was fabricated, as shown by optic photos in Fig. S10 (online). The current-voltage characteristics (*J-V*) for the champion cell measured under simulated solar AM 1.5 G irradiation (100 mW/cm^2) with forward and reverse scanning direction is given in Fig. 1i, revealing an open-circuit voltage (V_{oc}) of 0.668 V, J_{sc} of 22.283 mA/cm^2, and a fill factor (FF) of 0.590 under the reverse-bias scan, yielding PCE of 8.78%, the highest reported to date among single crystalline PSCs, to our best knowledge. The corresponding values under the forward scan were recorded as V_{oc} of 0.649 V, J_{sc} of 22.143 mA/cm^2, and FF of 0.572, respectively, resulting in a slightly smaller efficiency of 8.22%, and there is small hysteresis observed. Incident photon-to-current efficiency (IPCE) spectrums of selected single crystalline PSCs are shown in Fig. S11 (online), and the onset of IPCE photocurrent is redshifted to ~900 nm in comparison to polycrystalline PSCs, consistent with absorption spectra. The value is relatively low for wavelength from ~400 to ~780 nm, suggesting a lack of effective conversion in this range, and similar trend was reported for single crystal PSC by Dong et al. [3] The consequence is that the photocurrent integrated from area of IPCE spectrums is smaller than J_{sc} values measured from *J-V* curves, and such decrease of IPCE at shorter wavelengths was attributed to large defect density at interface, since shorter wavelengths generate carriers closer to the crystal surface [3]. Nevertheless, the other 9 devices tested have decent PCEs ranging from 6.14% to 8.21%, as shown in Table S1 (online) with selected *J-V* curves via reverse scans in Fig. S12 (online), where the maximum J_{sc} is observed to be 24.40 mA/cm^2.

Finally, we note that PCE of 8.78% is accomplished without full coverage of single crystalline $CH_3NH_3PbI_3$ on FTO/TiO_2 substrate, as observed from two SEM images in Fig. S5 (online). If completely covering FTO/TiO_2 substrate, then PCE of the single crystalline PSCs is expected to rise further, and there is still much room for improvement. With continuous optimization of materials processing and device optimization, and further understanding of the microscopic mechanism, we fully expect that single crystalline PSCs will rival their polycrystalline counterpart in the foreseeable future.

Table 1
Parameters that fits to the TRPL measurement based on double exponential equation. PC and SC refer to poly- and single-crystalline perovskites, respectively.

Sample	τ_1 (ns)	A_1 (%)	τ_2 (ns)	A_2 (%)	Avg. (ns)
FTO/PC	4.1	80.5	24.7	19.5	8.1
FTO/SC	64.0	51.3	356.1	48.7	206.2
FTO/TiO_2/SC	1.1	0.7	11.3	99.3	11.2

Conflict of Interest

The authors declare that they have no conflict of interest.

Acknowledgment

This work was supported by the National Key Research and Development Program of China (2016YFA0201001, 2016YFA0300804), the National Natural Science Foundation of China (11627801, 51102172, 51672007, 51502007, 11772207), the Leading Talents Program of Guangdong Province (2016LJ06C372), Shenzhen Science and Technology Innovation Committee (JCYJ20170307165905513, JCYJ20170413152832151), the Natural Science Foundation for Outstanding Young Researcher in Hebei Province (E2016210093), the Key Program of Educational Commission of Hebei Province of China (ZD2016022), and the Youth Top-notch Talents Supporting Plan of Hebei Province. This research used resources of the Advanced Photon Source, a US Department of Energy (DOE) Office of Science User Facility operated for the DOE Office of Science by Argonne National Laboratory under Contract No. DE-AC02-06CH11357.

Appendix A. Supplementary data

Supplementary data associated with this article can be found, in the online version, at http://dx.doi.org/10.1016/j.scib.2017.08.022.

References

[1] Stranks SD, Snaith HJ. Metal-halide perovskites for photovoltaic and light-emitting devices. Nat Nanotechnol 2015;10:391–402.

[2] Shi D, Adinolfi V, Comin R, et al. Low trap-state density and long carrier diffusion in organolead trihalide perovskite single crystals. Science 2015;347:519–22.

[3] Dong QF, Fang YJ, Shao YC, et al. Electron-hole diffusion lengths >175 μm in solution-grown $CH_3NH_3PbI_3$ single crystals. Science 2015;347:967–70.

[4] Zhang FY, Yang B, Mao X, et al. Perovskite $CH_3NH_3PbI_{3-x}Br_x$ single crystals with charge-carrier lifetimes exceeding 260 μs. ACS Appl Mater Interfaces 2017;9:14827–32.

[5] Liu YC, Ren XD, Zhang J, et al. 120 mm Single-crystalline perovskite and wafers: towards viable applications. Sci China Chem 2017. http://dx.doi.org/10.1007/s11426-017-9081-3.

[6] Wang GM, Li DH, Cheng HC, et al. Wafer-scale growth of large arrays of perovskite microplate crystals for functional electronics and optoelectronics. Sci Adv 2015;1:e1500613.

[7] Lee Lynn, Baek Jangmi, Park Kyung Sun, Lee Yong-EunKoo, Shrestha Nabeen K, Sung Myung M. Wafer-scale single-crystal perovskite patterned thin films based on geometrically-confined lateral crystal growth. Nat Commun 2017;8:15882.

[8] Chen Yao-Xuan, Ge Qian-Qing, Shi Yang, Liu Jie, Xue Ding-Jiang, Ma Jing-Yuan, Ding Jie, Yan Hui-Juan, Jin-Song Hu, Wan Li-Jun. General space-confined on-substrate fabrication of thickness-adjustable hybrid perovskite single-crystalline thin films. J Am Chem Soc 2016;138:16196–9.

[9] Rao HS, Chen BX, Wang XD, et al. A micron-scale laminar $MAPbBr_3$ single crystal for an efficient and stable perovskite solar cell. Chem Commun 2017;53:5163–6.

[10] Holger R, Tobias L, Michael JH, et al. Ferroelectric domains in methylammonium lead iodide perovskite thin-films. Energy Environ Sci 2017;10:950–5.

[11] Strelcov E, Dong QF, Li T, et al. $CH_3NH_3PbI_3$ perovskites: ferroelasticity revealed. Sci Adv 2017;3:e1602165.

[12] Stoumpos CC, Malliakas CD, Kanatzidis MG. Semiconducting tin and lead iodide perovskites with organic cations: phase transitions, high mobilities, and near-infrared photoluminescent properties. Inorg Chem 2013;52:9019–38.